

A PSEUDO MARKOV-CHAIN MODEL AND TIME-ELAPSED MEASURES OF MOBILITY FROM COLLECTIVE DATA

ALISHA FOSTER[†], DAVID A. MEYER[†], ASIF SHAKEEL[†]

ABSTRACT. In this paper we develop a pseudo Markov-chain model to understand time-elapased flows, over multiple intervals, from time and space aggregated collective inter-location trip data, given as a time-series. Building on the model, we develop measures of mobility that parallel those known for individual mobility data, such as the radius of gyration. We apply these measures to the NetMob 2024 Data Challenge data, and obtain interesting results that are consistent with published statistics and commuting patterns in cities. Besides building a new framework, we foresee applications of this approach to an improved understanding of human mobility in the context of environmental changes and sustainable development.

1. Introduction

Human mobility as a subject of analysis continues to grow with the advent, sophistication and proliferation of smart mobile devices, social networks, mobile applications and distributed services. Many of the models, and much of the analysis and computational work are based on data acquired as time and location of individual devices. This data is often collected from call data records (CDRs), information gleaned from trackers logging global positioning system (GPS) data, and from contextual and usage data from mobile applications. Under privacy concerns [1], the form of data considered appropriate for analyses has veered towards collective mobility data [2], with multiple levels of anonymization to resist individual identification [3, 4]. Such data present only aggregate information about the movements of groups, obscuring individual patterns of movement. Typically, the data is aggregated in both space and time: the geographical region the studied population resides in is divided into a grid, and the temporal span of the study is divided into a sequence of intervals. Combined by intervals and grid-cells, the aggregated data is made available as a time-series, giving for each time-step, ¹ the populations in cells, and counts and other statistics of trips taken between cells. Thus presented, the resulting data conceals information about the individuals, revealing only that about the collective.

The works of González, Hildago, and Barabási in 2008 [5] and of Barbosa, Barthelemy, Ghoshal, *et al.* in 2018 [6], describe models and measures of mobility stemming from individual mobility data. There are studies connecting random walks to human mobility patterns [7], and of trajectories and statistics of displacement [8] from individual mobility

[†]DEPARTMENT OF MATHEMATICS, UNIVERSITY OF CALIFORNIA, SAN DIEGO, LA JOLLA, CA 92093-0112, USA

E-mail address: a1foster@ucsd.edu, dmeyer@math.ucsd.edu, ashakeel@ucsd.edu.

Key words and phrases. collective mobility, measures of mobility, pseudo Markov-chain, machine learning, mobility models, urban, transportation, cell phone, anonymization, privacy, aliasing, efficiency and sustainability from mobility data.

¹Depending on the context, we will interchangeably say time-step or interval.

data. We are interested, in this paper, in understanding the longer term flows resulting from collective mobility, the kind of interpretable patterns that result from them, and in determining their efficacy and utility for estimating criteria for guided decision-making. Applications could range from comparative studies, to planning and forecasting based on these criteria and measures. Thus, an objective of this paper is to extract measures of mobility akin to those developed for individual mobility tracked over longer times [6], but now from collective mobility data, with de-facto privacy. For each interval in the time-series, the basic aggregated information usually consists of the count of devices detected in each geographical cell and the observed number of trips between pairs of cells, from each pair’s *origin* (O) to its *destination* (D) cell. Supplementing that basic information to enable physically meaningful analysis, additional summary statistics of quantities such as the mean distance or time of travel between the pairs of cells may also be in the data. To increase the level of anonymization, coarsening of the data may extend to the counts of population and trips, with those below a threshold being omitted, as in the data we study, the NetMob 2024 Data Challenge [9] data.

Various aspects of human movements are captured by measures described in [5, 6, 10], among them *jump-length*, *radius of gyration*, *mean-squared displacement* derived from individual mobility data of long-term movements. Instead, we are interested in eliciting similar measures from collective data with anonymized, aggregated trip-counts between coarse-grained locations and over intervals that may or may not be aligned with the dynamics of the population movements. Such measures may qualitatively describe the patterns of movements and quantitatively provide simple social and economic mobility indicators summarizing underlying complexities and modes of movement, and interactions between intrinsic structures and extrinsic forces. The aim is to develop these criteria and measures to be further used as deemed useful in dynamic analyses of mobility and its effect on the environmental factors, livability, efficiency and sustainability of communities, and vice-versa [11–13]. Studies of relationship between short-term and long-term mobility exist [14], as well as those of collective mobility [15–18], but the questions posed and the analyses conducted are fundamentally different from those motivating and addressed in the model we develop.

Our analysis uses the mobility datasets from the NetMob 2024 Data Challenge [19]; the details of the data are in the document “The NetMob2024 Dataset: Population Density and OD Matrices from Four LMIC Countries” [9].² The data are provided by Cuebiq.³ These datasets include data from the following countries: Mexico, Indonesia, India, and Colombia. All of the data is already aggregated and is provided at several resolutions: spatially by a grid whose cell geometry and resolution (cell size) is given by one of the geohash levels: GH3, GH5, or h37, and temporally by one of the time intervals: 3-hourly, daily, weekly, or monthly. A *location* is taken to be the centroid of a cell.⁴ For a given country and aggregation, the

²LMIC: Low and Middle Income Countries.

³Cuebiq’s terms and conditions for the NetMob 2024 Data Challenge require us to refer the reader to the following statement pertaining the availability of data: “Aggregated data was provided by Cuebiq Social Impact as part of the Netmob 2024 conference. Data is collected with the informed consent of anonymous users who have opted-in to anonymized data collection for research purposes. In order to further preserve the privacy of users, all data has been aggregated by the data provider spatially to the GH3, GH5, h37 and temporally to 3-hourly, daily, weekly, and monthly levels and does not include any individual-level data records.”

⁴The centroid of a cell in turn identifies the cell uniquely as the cell boundaries are fixed by the geohash chosen.

population data is given as a time-series of the location (cell) population counts, and the *OD data* as a time-series of trip-counts for the origin-destination (OD) pairs of locations (cells). As mentioned above, the data in both cases are omitted if the respective count is below the threshold of 10. The OD data, along with the trip-counts, include the means, the medians and the standard deviations of the distances traveled (trip-distance) , ⁵ and of the times of travel (trip-time) for each OD pair. All the calculations in this paper are for 3-hourly GH5 OD data for the year 2019.

This paper is organized as follows. In section 2 we describe the data in generic terms and set up the pseudo Markov-chain model. We use the OD trip-count data to construct the model, under the assumption that the individuals in the data are indistinguishable. This allows a probabilistic description of an individual whose probability of transition from an origin to a destination in any time-step is approximated by the trip-count normalized by the total number of trips emanating from the origin. We call this description of an individual a *privacy enhanced person* (PEP). A PEP's inter-location transitions thus become a Markov (Stochastic) transition matrix. Chaining the time-steps as successive transition matrices, we obtain a *time-elapsd* version of a PEP. In the process, we identify what we term *mobility-aliasing*: counting the same individuals as part of successive OD trips, as a side effect of using too long an interval for aggregation. This issue could possibly be addressed in two ways. First, by an appropriate strategy based on movement speeds when initially aggregating the data spatio-temporally. Second, by post-processing through algorithmic means to approximate the roots of the original transition matrices in the cases such as Netmob 2024 where the data has been aggregated at space and time scales that are pre-determined. In some sense this is the reverse of the pseudo Markov-chain model, and underlines the flow of ideas from a mathematical domain to mobility research as the authors of [20] recommend. This level of aggregation would make the estimates more reflective of the true dynamics of mobility. Given the size of matrices we are dealing with in this paper, it was not efficiently computable with the computing resources available, but is a topic for future research. We also set aside the notion of *waiting-time* between stops, referred to in [6]. For the current investigation, we use the original matrices to demonstrate the machinery and the usefulness of the measures.

In section 3 we develop the first extension of the Markov-chain [21] formalism. This is a calculation of the time-elapsd OD net trip-counts (net flow). We validate this for Mexico City area, for the morning and afternoon of a randomly selected day, which show that the main directions of population movements are consistent with daily commuting. We surmise that over longer time and distance scales and more detailed data, such net flow calculations might show patterns of migration related to climate and environmental shifts.

In section 4 we seek a measure of time-elapsd travel that may sense the presence of inefficiencies in travel patterns, arising from routing constraints, detours, congestion, or other impediments. First, we calculate the time-elapsd origin-to-destination distance traveled by a PEP for a generic OD pair. This is a weighted mean over multiple possible paths taken by a PEP over consecutive time-intervals, and we use the Markov structure to develop a recursive algorithm for it. Then we address the issue of estimating the most direct OD trip-distance as a baseline to compare with the time-elapsd OD distance. We normalize the time-elapsd OD distance by the direct trip-distance estimate to arrive at the dimensionless measure we

⁵The mean distance traveled may be shorter or longer than the geographical distance between the origin and destination locations, i.e., cell centroids.

call the *effective distance*. An OD pair can be tracked for its effective distance over time, and different OD pairs can be compared with each other by their respective effective distances. We compute and plot the morning 6-hourly effective distances of all OD pairs in Mexico City area against dates in 2019. That helps us identify OD pairs with high effective distances and the days on which they occur. We display the more significant examples of these on maps as a visual confirmation: the OD pairs and the effective distances between them, as well as the indirect paths responsible for the cumulative distances. We observe both spatial and temporal persistence of such OD pairs, and note that measures of persistence or flow-based characterizations of such constellations might be possible. We could calculate the equivalent for the trip-time, but we only illustrate the concept with the trip-distance.

In section 5 we propose measures that could be construed in the sense of the radius of gyration [6]. Radius of gyration [5] is a measure of the typical distance traveled by an individual. It has variants refining that notion [6]. Our collective mobility counterparts to it are the return-to-origin (RTO) distance, time and speed measures. RTO distance and time, as the names imply, are the mean distance and time a PEP travels in returning to the place of origin over some fixed duration. RTO speed, instead, is a pseudo-speed defined simply as the ratio of RTO distance to RTO time. It cannot be directly interpreted as the conventional speed. We plot the RTO measures for Mexico City, Jakarta, and Mumbai against dates in 2019. Comparing among them we find trends that reflect shared characteristics and differences that may ultimately have roots in their modes of life, social and economic activities, seasonal and environmental effects, and infrastructure and transportation networks.

Section 6 is the conclusion and discussion of the results and future research.

2. Pseudo Markov-chain Model

To construct the pseudo Markov-chain model, we assume that individuals, as far as their movements are concerned, are indistinguishable. In particular, their probability of transitioning from one location to the next at any time-step is independent of their history of transitions. Thus, they provide typical realizations of a Markov process, i.e., one characterized by the memoryless property. We adopt the term *privacy-enhanced person* (PEP) when we refer to an instance of this randomized individual traversing a path over the grid locations.

We construct a stochastic matrix M^t which encodes the probabilities of transitioning to a destination given an origin location at a single time-step t . In order to extend our inferences from single time slices to multiple sequential time slices, we create a *time-elapsing transition matrix* A^t which gives the transition probabilities to a destination given an origin location over a time interval *up to* time-step t . We use these time-elapsing matrices and additional information to make longer term inferences from the data—estimating the net population movement over time, mean distance traveled over time, and the average amount of time it takes for a person to return to their origin location.

Depending on the space-time resolution chosen, the trips might mostly begin and end between locations in the vicinity of major city-centers (3-hourly GH5) or among far-away regions (daily, GH3). It makes sense then to be concerned with connected-components, at time-scales of interest, and not the entire country. The model is constructed from the data, so we describe the data in general terms.

2.1. *Generic Data Description.* The data we will be using to construct the model and compute with is part of the Netmob 2024 Challenge data. It contains two types of datasets:

population data and OD trip data. We use the OD trip data in this paper. It is aggregated in time by intervals (time-steps) and in space by grid cell identified by their centroid given as a geohash location. Each trip is indexed by the triple: (time-step, starting geohash location, ending geohash location). The resolution of time-steps could be 3 hours, a day, a week, or a month. Geohashes could be GH5 (4.9km side-length, square grid), GH3 (156.5km side-length, square grid), or h37 (1.41km side-length, hexagonal grid). We will only use the 3-hourly, GH5 data for the year 2019 for computations.

Trip data are aggregated such that only trips starting and ending in the same time-step are recorded. For each index point, the fields include trip-count (number of trips in the interval), mean/median/standard-deviations of trip distance of travel (m), trip duration/time of travel (min), and other quantities that we are not going to be utilizing in this paper. In any time-step if an OD pair has a trip-count below the threshold of 10, that OD pair is omitted. It may be that the same individual is part of several successive trips within a time interval or in consecutive time intervals. Thus, there is no expectation that the trips between different pairs of locations (in particular pairs that are adjacent geographically) within the same time-step are for different individuals.⁶

For each time-step, the trip data can be represented as a directed graph with edges weighted by the trip-count.⁷ In order to extend these shorter-term data to longer-term movements and to develop interesting measures, we organize the trip data into a pseudo Markov-chain model. The multiple-step intervals and the measures that we estimate over their duration will be called *time-elapsed*.

2.2. Model construction. For the purpose of this discussion, consider the time-series of trip-counts for a country over some finite sequence of time-steps $t = 1, \dots, n$. Let there be N locations in the country. There are thus N^2 potential directed edges (origin-to-destination direct paths, which we refer to as OD pairs) in the graph of trip data at any time-step. Normally, this graph is sparse. We mainly work with the strongly-connected components⁸ of the graph for two reasons: first is that it defines areas that are actively connected by routes, and second is that Markov (transition) matrices constructed on strongly-connected components have desirable properties such as no pure absorbing or reflecting nodes.

We first extend the idea of a graph at a time-step to all the time-steps occurring within some time-elapsed interval ending at time-step T . Let $E^t = \{(i, j)^t\}$ (where $i, j \in 1, \dots, N$) be the set of edges that appear in time-step t . Let $E_T = \cup_{t=1}^T E^t$, be all the edges that appear in the intervals up to time-step T . Consider the strongly-connected components of the graph given by the edges in E_T on the set of all locations. Let C be one such component of size $N_C = |C|$. Label the set of locations in C by $i = 1, \dots, N_C$.

Let the trip-count from location j to location i in C at time-step t be f_{ij}^t . Assume that for each origin $j \in C$ and each time-step t , there is at least one destination $i \in C$ such that $f_{ij}^t \neq 0$, i.e., every origin has at least one outgoing trip, including trips to itself (which we will

⁶In the course of this work, we found that mean trip distances provided in the data often have very large values (compared to geographical distances), indicating anomalies or issues with the data collection mechanism. We chose to use median trip-distances as they avoid being influenced by a few such very high values, which are likely incorrect.

⁷A recent paper [18] on massive datasets for Mexico constructs daily weighted directed graphs as well, but their analysis is in a different direction.

⁸For the reader unfamiliar with graph terminology, a strongly-connected component of a directed graph is one in which there is a directed path from every node to every other node.

often refer to as self-transitions).⁹ Then the estimated probability of the trip to destination i given that the origin is j , at time-step t , is

$$m_{ij}^t = \frac{f_{ij}^t}{\sum_{i=1}^{N_C} f_{ij}^t}.$$

The denominator in the above expression, $\sum_{i=1}^{N_C} f_{ij}^t$, is an estimate for the number of individuals at location j at the beginning of time-step t . The one-step transition matrix is then

$$M^t = [m_{ij}^t]. \quad (1)$$

For the remainder of the discussion, assume that C is a maximal component, and every summation has lower limit 1 and upper limit N_C , unless indicated otherwise.

Further assume that the Markov property holds for trip-counts: for any t , trip-counts $f_{i'j'}^t$ and $f_{i''j''}^{t'}$ for any $t' < t \leq t''$, and for any i', j', i'', j'' , are independently distributed. Then, the transition probability to destination i given the origin j , a_{ij}^t , during the interval up to time-step t is given by:

$$A^t = [a_{ij}^t] = \prod_{k=1}^t M^k = M^t A^{t-1}, \quad t \geq 1, \quad (2)$$

where $A^0 = \mathbb{I}$, the identity matrix.

Before going further, we describe a concern regarding the time intervals for aggregation, which affects the predictions and estimates based on this model.

2.2.1. Mobility-aliasing. The second assumption in our pseudo Markov model is that an individual only moves one cell per the time-step. Let us consider this and examine some relevant issues.

We take the case of 3-hourly GH5 data. The mean *speeds*¹⁰ of travel between locations (excluding trips in the same cell, i.e., self-transitions) as calculated from the data are, for Mexico City (Mexico): 127 m/min, Jakarta (Indonesia): 125 m/min and Mumbai (India): 100 m/min (based on median trip distances and times). GH5 locations, by the data description document [9], have a spatial resolution of 4.9 km. This implies that about 45 minutes are required to travel between adjacent locations for any of these countries. That would allow 4 or more transitions to happen in a 3 hour interval for each individual. In other words the time resolution of the data is far coarser than required by the speed of the movements.

A consequence of the above is that an individual could be observed in several consecutive locations in the same time-step, i.e., be counted in trips between different locations in the same time-step. This is what we term, by analogy to a phenomenon in time-frequency analyses, *mobility-aliasing*. To minimize this aliasing, finer time-resolution would be required. We propose a data collection scheme to reduce mobility-aliasing and propose an algorithmic workaround in appendix A. Recognizing that the algorithmic compensation we

⁹In the Netmob 2024 data there are time-steps for which some of the origin locations $j \in C$ have all the f_{ij}^t missing, possibly because there is a cut-off for fewer than 10 trips. Currently, we make the reasonable, though inaccurate, amendment of adding $f_{jj}^t = 5$ (midway between 0 and 10) for such j , creating self-transitions with probability 1 for such locations and time-steps.

¹⁰Not having the data for speed of travel between locations, we take *speed* as the median distance traveled divided by the median time of travel for each time-step and each OD pair whose origin and destination are distinct. Then, we take the average of these speeds over all the pairs weighted by the trip-counts.

proposed is currently not efficiently computable for the size of matrices involved, with the resources we have, we continue our development and assume that a PEP moves at the original time intervals. This allows us to calculate further, and still illustrate the salient features of the methodology. In the following, we develop time-elapsd measures of mobility that are calculated from the distances or times of travel from the OD data.

3. Time-elapsd origin-destination trip-counts (net flows)

In this section, we build on the model to calculate the time-elapsd net flows (trip-counts) between locations. Simply put, starting with the total out-going trips from each origin at the beginning of a time-elapsd interval, we estimate the *net* number of trips between each OD pair over that interval.¹¹

3.1. *Derivation.* The formalism below defines a function to properly weight each edge and then computes the net trip-count as a difference weighted by edge probabilities. For each OD pair, i.e., edge (i, j) , we define the movement function over the OD pairs (edges) in $(k, l) \in C$ at time-step t :

$$s_{kl}^t(i, j) = \delta_i(k)\delta_j(l) - \delta_i(l)\delta_j(k).$$

Since (i, j) is fixed, this can be viewed as a matrix indexed by pairs $(k, l) \in C$, with values 1 at index (i, j) , -1 at index (j, i) , and 0 elsewhere.

Let the set of ordered edges in C be

$$E^o = \{(i, j) \mid i < j \in C\}.$$

The probability of a generic individual being at location j at time-step $t = 1$ is estimated as

$$p_j^1 = \frac{\sum_i f_{ij}^1}{\sum_{i,j} f_{ij}^1}, \quad (3)$$

and that of a generic individual moving from j to i over the time-elapsd interval including the time-step t , in terms of the entries of the matrix A^t in equation (2), is

$$p_{ij}^t = p_j^1 a_{ij}^t$$

The total count of individuals summed over all locations at time $t = 1$ is

$$n^1 = \sum_{i,j} f_{ij}^1$$

The total count of individuals at time $t = 1$ at location j is

$$n_j^1 = \sum_i f_{ij}^1 = n^1 p_j^1.$$

¹¹The reader may choose to skip the derivations, and read the results sections to get the main ideas through plots, maps and descriptions.

Then the mean time-elapsd count of individuals moving from j to i , the *net trip-count* function \bar{s}^t , over E^o at time-step t , is

$$\begin{aligned} \bar{s}^t : E^o &\rightarrow \mathbb{R} \\ \bar{s}^t(i, j) &= \sum_{k,l} s_{kl}^t(i, j) n^1 p_{kl}^t \\ &= n^1 (p_{ij}^t - p_{ji}^t) \\ &= n^1 (p_j^1 a_{ij}^t - p_i^1 a_{ji}^t) \\ &= a_{ij}^t n_j^1 - a_{ji}^t n_i^1. \end{aligned}$$

Here, positive values of $\bar{s}^t(i, j)$ are net trip-counts from j to i and negative values are net trip-counts from i to j .

3.2. Results. We validate the net trip-counts (net flows) by computing commuting flows into (and out of) Mexico city-center during the 3:00–6:00–9:00–12:00 and 15:00–18:00–21:00–00:00 sequence of 3 hour intervals (9 hours time-elapsd intervals), on a randomly chosen date (06-05-2019). These net trip-counts are shown on the maps in figures 1a, 1b, which show the top 0.95, 0.95 quantiles of net trip-counts for the respective intervals. The flows are from the periphery to the center in the 3:00–6:00–9:00–12:00 in and and vice-versa in the 15:00–18:00–21:00–00:00 interval. Magenta-colored end of the scale is the lower end of the quantile, and navy-colored is the higher end. The estimated trip-counts are an order of magnitude different between figures 1a and 1b because the original dataset records are of the same order, i.e., the total starting trip-count for 3:00–6:00 is an order of magnitude smaller than for 15:00–18:00.¹² Most of the transitions (which are larger) are within the same geohash location, i.e., self-transitions, which are not shown here, and have a 0 net trip-count by definition.

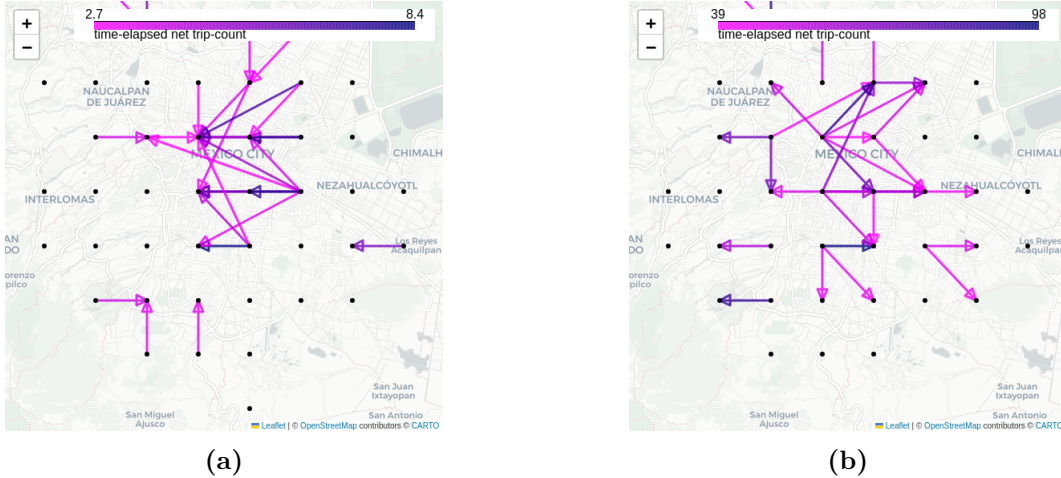


Figure 1. Mexico City, 06-05-2019, net trip-counts (a) 3:00–6:00–9:00–12:00 triple of 3-hour intervals. Top 0.95 quantile. (b) 15:00–18:00–21:00–00:00 triple of 3-hour intervals. Top 0.95 quantile.

¹²The starting total trip-count for each interval includes any default self-transitions that had to be included for locations in the maximal component that were missing in the starting interval.

We can compare these flow maps with single time-step maps at the start of the respective time-elapsed intervals. The maps in figures 2a and 2b are the flow maps for 3-hour intervals 3:00–6:00 and 15:00–18:00, respectively. Generally, the flows are directed as they are in the corresponding time-elapsed 9-hour intervals. However, there appears to be a consolidation of flows in the maps of figures 1a and 1b and higher degree of directionality compared to the single time-step flows of figures 2a and 2b.



Figure 2. Mexico City, 06-05-2019, net trip-counts (a) 3:00–6:00 interval. All. (b) 15:00–18:00 interval. Top 0.9 quantile.

This validation at the scale of a city suggests that net flow calculations at a larger spatio-temporal scale with more detailed data might show migrations related to seasonal effects, climate change and environmental challenges.

4. Time-elapsed origin-destination distance traveled and effective distance

We build further and estimate the mean time-elapsed origin-to-destination distance traveled by a PEP for all OD pairs (some of which may or may not be in the data). We must keep track of the accumulated distances along all allowed intermediate paths for this purpose. The Markov property enables us to find a recursive algorithm to calculate this time-elapsed travel distance from the trip-distance in the data for the intermediate time-steps and OD pairs.

The time-elapsed OD distance, when significantly longer than expected for an OD pair, perhaps means circuitous paths are more active than the most direct available. To be useful as an indicator of higher than expected travel distance, it would need to be compared to an expected/baseline direct OD distance for that OD pair. That baseline may be found from the data as an expected distance for that pair if the data contains it, otherwise it would need to be imputed from the geographical origin-to-destination distance for the OD pair. We normalize the time-elapsed OD distance by its baseline distance, calling it the OD pair’s *effective distance* for the time-elapsed window. OD pairs can be compared by their effective distances over the same time-elapsed window. Tracked over time, this may help in finding the OD pairs with consistently longer than expected travel distances due to, among other reasons, bottlenecks or other circumstances necessitating diversions. Were we to substitute in this description travel-time for travel-distance, we may then be comparing the routes that

are more time-consuming or time-efficient than others. We only consider travel distances in this paper.

4.1. *Derivation: time-elapsd OD distance traveled.* For the origin j and destination i , we keep track of the mean distances for all time-elapsd paths from j to all intermediate locations k that have not passed through i, j except at the beginning ($t = 0$). Let us call such path distances $y_k^{i,j,t}$, taking $y_k^{i,j,0} = 0$. Here we think of $\mathbf{y}^{i,j,t} = [y_k^{i,j,t}]$ as a one-dimensional vector. In the following the superscripts i, j are simply to keep track of the particular OD pair under consideration. They are not useful in the calculations of mean distance and can be safely ignored.

We define a vector $\mathbf{p}^{i,j,t} = [p_k^{i,j,t}]$, recursively as follows. Let $\mathbf{p}^{i,j,1} = [m_{kj}^1]$, the j -th column of matrix M^1 in equation (1). Let

$$p_k^{i,j,t} = \sum_{r|r \neq i,j} m_{kr}^t p_r^{i,j,t-1},$$

for $t \geq 2$. We can write this a matrix operation by defining a vector in terms of $\mathbf{p}^{i,j,t}$ with i, j entries set to 0:

$$\tilde{\mathbf{p}}^{i,j,t} = [\tilde{p}_k^{i,j,t}],$$

where

$$\tilde{p}_k^{i,j,t} = \begin{cases} p_k^{i,j,t}, & \text{if } k \neq i, j \\ 0, & \text{otherwise} \end{cases}$$

Then,

$$\mathbf{p}^{i,j,t} = M^t \tilde{\mathbf{p}}^{i,j,t-1}.$$

Let the (median) distances, from the data, traveled between locations for time-step t , for each (i, j) , be d_{ij}^t . Then,

$$\begin{aligned} y_k^{i,j,t} &= \frac{1}{\sum_{r|r \neq i,j} m_{kr}^t p_r^{i,j,t-1}} \sum_{r|r \neq i,j} (d_{kr}^t + y_r^{i,j,t-1})(m_{kr}^t p_r^{i,j,t-1}) \\ &= \frac{1}{p_k^{i,j,t}} \sum_{r|r \neq i,j} (d_{kr}^t + y_r^{i,j,t-1})(m_{kr}^t p_r^{i,j,t-1}), \end{aligned}$$

with probability $p_k^{i,j,t}$. We can organize the above computation as matrix operations. Define a matrix

$$\tilde{D}^{i,j,t} = [\tilde{d}_{kr}^{i,j,t}],$$

where

$$\tilde{d}_{kr}^{i,j,t} = \frac{d_{kr}^t + y_r^{i,j,t-1}}{p_k^{i,j,t}}.$$

Then we can write:

$$\mathbf{y}^{i,j,t} = [\tilde{D}^{i,j,t} \cdot M^t] \tilde{\mathbf{p}}^{i,j,t-1},$$

where the \cdot in the above is the element by element multiplication, followed by the usual matrix product.

Let us simplify notation and denote by x_{ij}^t the mean distance traveled from j to i for paths ending at time-step t that have not passed through i, j except at the beginning, which in terms of $y_k^{i,j,t}$ is

$$x_{ij}^t = y_i^{i,j,t},$$

and denote the probability of that path by π_{ij}^t ,

$$\pi_{ij}^t = p_i^{i,j,t}.$$

The mean distances of paths from j to i that end between $t_1 \leq t \leq t_2$ in terms of this notation is,

$$\bar{x}_{ij}^{t_1,t_2} = \frac{\sum_{t=t_1}^{t_2} x_{ij}^t \pi_{ij}^t}{\sum_{t=t_1}^{t_2} \pi_{ij}^t}. \quad (4)$$

Note that replacing travel distance by travel time for each step, we can obtain the mean time taken from j to i .

Time-elapsed distances between OD pairs over time-elapsed intervals spanning more than a single time-step, as in the case of net trip-count above, estimate the distance traveled between locations as a weighted mean of allowed intermediate path trip-distances over multiple paths, weighted by the relative path probabilities. Allowed paths are the ones that leave the origin at the beginning and end at the destination, without passing through either at any other intermediate time-step.

4.2. Normalization: time-elapsed OD effective distance. The utility of a distance measure, since it accounts for the direct and the indirect paths for each OD pair, might lie in providing a proxy for deviation from the most direct path. Note that each OD pair has a natural geographical distance between its origin and destination associated with it.¹³ Geographical distances are different for different OD pairs; so is the time-elapsed distance. Two OD pairs cannot, therefore, be compared by their time-elapsed distances, with the intention to find the one with higher potential deviation. Hence the need for normalization of the time-elapsed distance for each OD pair by a base distance for that pair.

There are two natural candidates for the base distance of an OD pair. First is the OD geographical distance. Adopting this as the base for comparison runs into an issue: the mean (or median in our case) trip-distance provided for the same OD pair varies from time-step to time-step, nor is it consistent relative to the geographical distance. It may be longer than the geographical distance or shorter depending on the time-step. Indeed, it is not directly reflective of the local geography of travel, which is rarely in a straight line.

The other obvious candidate as the base distance for an OD pair is an appropriate mean of the trip-distances for that pair over the entire time series. This is derived from, and directly reflective of the local geography, characteristics and modes of travel. Here, we have the issue that not all pairs of locations that can result from time-elapsed movements are available in the data.

To accommodate both the issues, we impute the base distances. First, note that the trip-distances and the geographical distances are correlated. We obtain, through linear regression using weighted (by trip-counts) mean squared error (MSE), the line of best fit between the geographical distances (as the independent variable) and the median trip distances from data (as the dependent variable). Using this relation, we can estimate the base OD pairwise trip distances from their geographical distances. We now have an estimate of the base trip-distance/standard-deviation, which is the mean standard-deviation of the OD trip-distance over the entire time-series, when that OD pair is in the data, or the estimated distance/root mean-squared error (RMSE) from the regression when it is not. We can now normalize the

¹³This can be calculated from the origin and destination (longitude, latitude) pairs determined by their geohashes.

time-elapsed distance for each OD pair by its base distance plus standard-deviation (to be conservative), and call it the *effective distance*. This normalization allows a comparison of any two OD pairs by their effective time-elapsed distances.

For the regression, we do not keep self-transitions, since we are interested in OD pairs which have distinct origin and destination. Figure 3 shows the regression for Mexico City and surrounding areas (up to 10 km zone around Mexico City). Although the intercept is *negative*, we still use it for regression because it is seen as a nonlinear fit approximated by a linear fit. The line of fit is a crude fit at best, though it matches the overall trend. We will not obtain negative estimates for the base trip-distance because by the nature of GH5, minimum geographical distance would be about 4.9 km, which ensures a positive estimate for the base distance. The data appears in clumps of trip-distances for each origin-to-destination geographical distance, since the latter are a finite number of values based on the grid. There is high variance in each cluster, which indicates that a single independent variable is likely not the best choice and that the model is too simplistic. A better model would take into consideration the geography and employ a more sophisticated set of independent variables to perform the regression. That is to be expected, as the terrain, nature of physical structures, routes, means of transport, and socio-economic conditions vary widely among the locations that are otherwise at the same geographical distance. Our intent is to provide a baseline method which can be expanded upon.

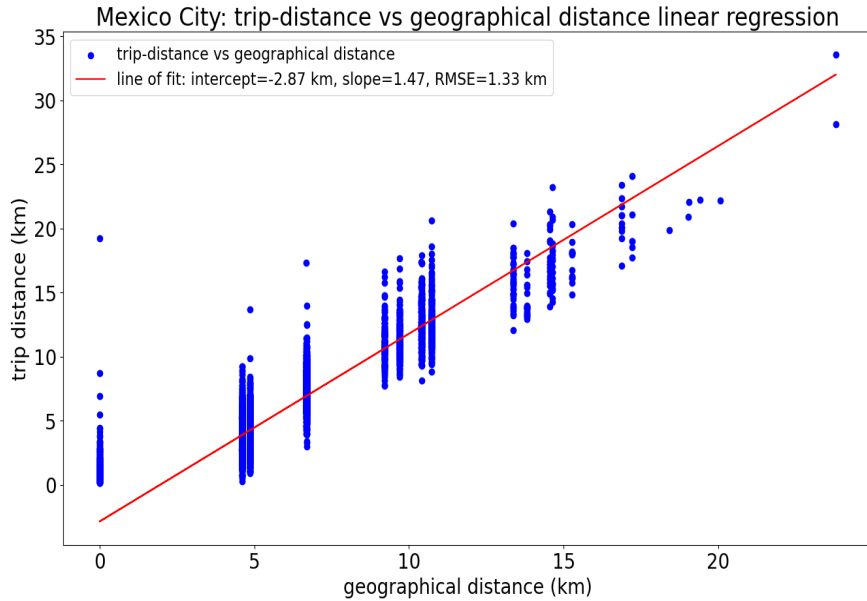


Figure 3. Mexico City: Linear fit of the trip-distance to geographical distance.

4.3. *Results: time-elapsed OD effective distances.* From previous sections, we know that a PEP travels in a manner that changes with the time of the day. We consider the morning time to calculate the time-elapsed effective distance. Figure 4 is a scatter-plot of the effective distances for the time-elapsed interval 6:00–9:00–12:00, for each day in 2019.¹⁴ We only show those OD pairs that are in the top 0.95 quantile of the effective distances for that day. Each

¹⁴We use a staged method to calculate the mean trip-distance for the OD pairs which are in the data. For a given time-elapsed interval (including the date), for instance 06-05-2019, 6:00–9:00–12:00, we first look in that dateinterval for the OD pair and calculate its trip-distance mean. Absent that, we check that

OD pair has a color corresponding to it.¹⁵ The legend shows the OD pair, its color in the scatter plot, and the frequency in days on which the OD pair is in the top 0.95 quantile of effective distances. Only a partial legend is visible, since the number of OD pairs is large.

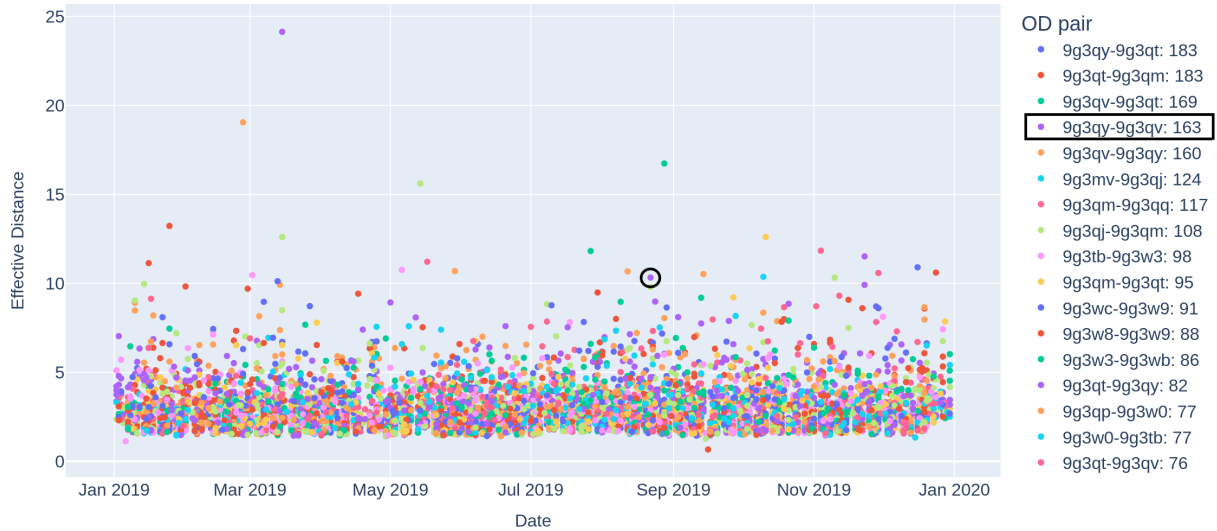


Figure 4. Mexico City, daily, 6:00–9:00–12:00: time-elapsed effective distances of OD pairs. Top 0.95 quantile per day. Legend shows the frequency of occurrence in days of the OD pairs. Circled: on 08-22-2019, OD pair (9g3qy,9g3qv) with effective distance 10.2.

From the plot above, 08-22-2019 has a high effective distance value of 10.2, circled in black. This corresponds to the OD pair whose GH5 coordinates are (9g3qy,9g3qv).¹⁶ For this date, as a further illustration, we show on the map in figure 5a the effective distances of OD pairs for trips in the time-elapsed interval 6:00–9:00–12:00, above quantile 0.985. At this quantile, Figure 5a reveals the effective path for the mentioned OD pair circled in black (navy-colored arrow, upper middle). A possibility is that it indicates a tendency to travel on more indirect paths between the origin and destination, picked up by the time-elapsed estimate. The same OD pair occurs 163 days out of the year with a high effective distance. Underlying reasons, when such high effective distances are observed, would need further study.

time-elapsed interval(here 6:00–9:00–12:00) and the same weekday as the original date (06-05-2019 was a Wednesday) in all the weeks. Next we search all the days in the data, still for the same time-elapsed interval. Finally, we try the entire dataset for that OD pair regardless of the time-elapsed interval.

¹⁵Due to limitations of colored plotting, different pairs may correspond to the same color.

¹⁶Hereon, we will refer to locations by their GH5 geohashes, leaving out the geohash level.

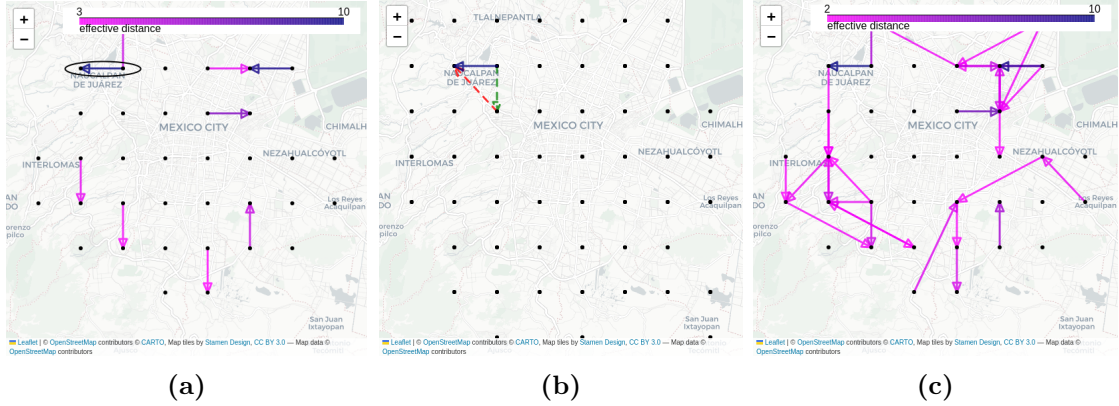


Figure 5. Mexico City, 08-22-2019, time-elapsed effective distances of OD pairs (a) 6:00–9:00–12:00: Top 0.985 quantile. (b) Actual path as single-interval segments: dashed green arrow is the outgoing segment from the origin (9g3qy) during 6:00–9:00; dashed red arrow is the incoming segment to the destination (9g3qv) during 09:00–12:00. (c) 6:00–9:00–12:00: Top 0.95 quantile.

We can also decompose the OD pair into path segments that contributed to the time-elapsed trip. Figure 5b shows the single time-step trips. The dashed green arrow is the segment leaving the origin (9g3qy) in the interval 6:00–9:00, and the dashed red arrow is the segment entering the destination (9g3qv) in the interval 9:00–12:00. This decomposition makes it clear how the path acquired a high effective distance. In this example, a single two-segment path over two intervals contributed to the longer-than-expected path distance. The OD pair could have a direct path in which is much shorter than the two-segment path. That would make the occurrence of a long path such as this, be very abnormal.

Let us relax the threshold and see if these high effective distance pairs fall in a broader pattern. We reduce the quantile cut-off to 0.95 and show the time-elapsed effective distances in figure 5c for the same time-elapsed interval. We observe that the mentioned OD pair is part of a set of high effective distance OD pairs. This points to the possibility of studying effective distances as part of spatially persistent patterns, within the purview of topological data analysis (TDA) [22].

As emphasized earlier, this is a demonstration of the methodology, and as such, we also take a look at those OD pairs which are not in the original data, but developed a path over successive time-steps. We call such pairs *globally-unconnected* OD pairs. Figure 6 is the scatter-plot, for days in 2019, of the effective distances of globally-unconnected OD pairs for trips in the time-elapsed interval 6:00–9:00–12:00. The plot only shows pairs above quantiles 0.95. Generally, the effective distances of such pairs are lower, because this is a restricted set. The normalization here is purely regression-based, since the OD pairs are not in the data. Recall that the normalization is not simply by the regression-obtained trip-distance, but by the sum of that with the standard-deviation (RMSE) of the fit. From the plot, 09-23-2019 has an OD pair with a high effective distance value of 2.16, circled in black. This corresponds to the OD pair (9g3w6,9g3w0). The same OD pair appears with a high effective distance on other days as well, 108 times during the year.

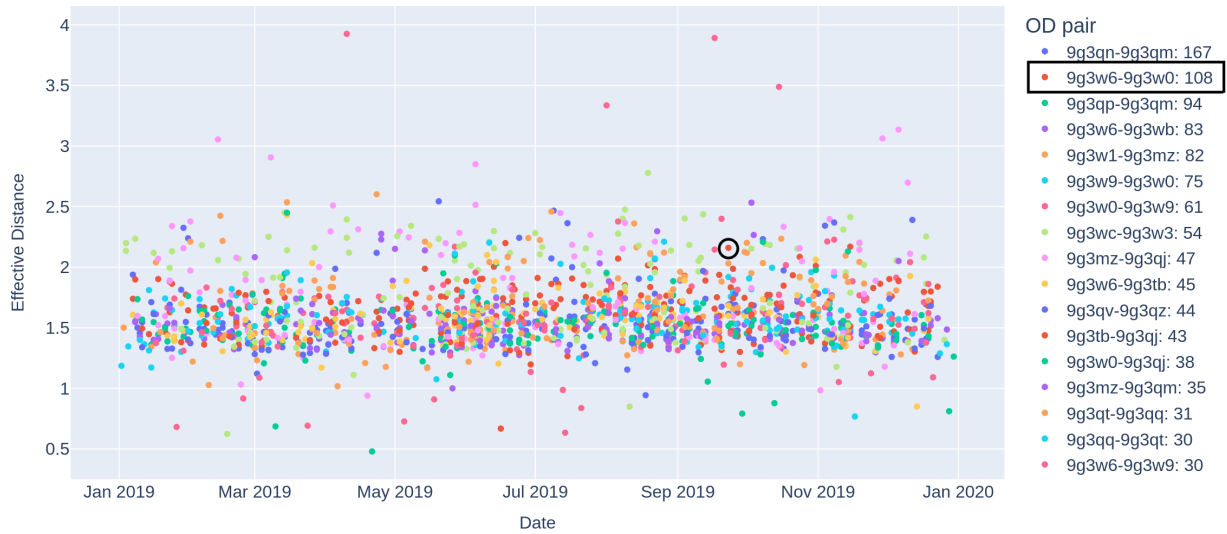


Figure 6. Mexico City, daily, 6:00–9:00–12:00: time-elapsd effective distances of globally-unconnected OD pairs. Top 0.95 quantile per day. Legend shows the frequency of occurrence in days of such OD pairs. Circled: on 09-23-2019, OD pair (9g3w6,9g3w0) with effective distance 2.16.

Figure 7a is the map showing effective distances above quantile 0.985. The effective path for the mentioned OD pair (9g3w6,9g3w0) is circled in black (navy-colored arrow).

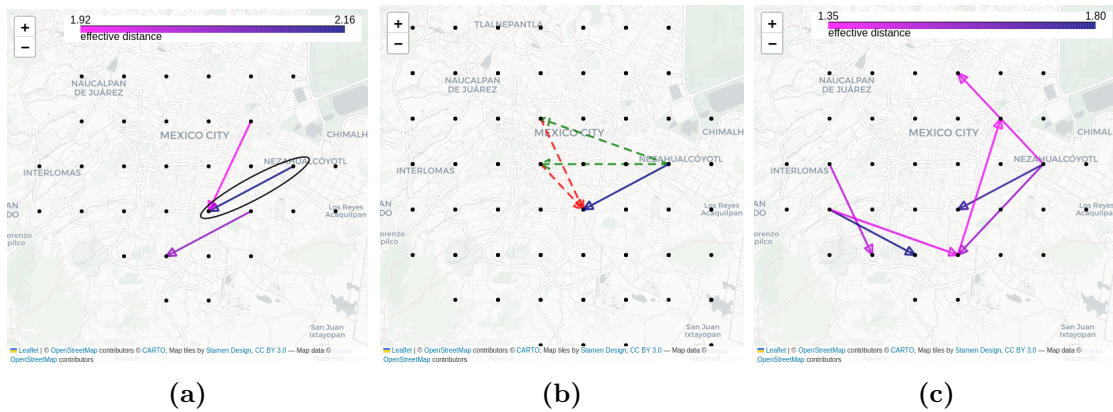


Figure 7. Mexico City, 09-23-2019, time-elapsd effective distances of globally-unconnected OD-pairs (a) 6:00–9:00–12:00: Top 0.985 quantile. (b) Actual paths as single interval segments: dashed green arrows are the outgoing segments from the origin (9g3w6) during 6:00–9:00; dashed red arrows are the incoming segments to the destination (9g3w0) during 09:00–12:00. (c) 09:00–12:00–15:00: Top 0.95 quantile.

As before, we decompose the OD pair into path segments that contributed to the time-elapsd trip. Figure 7b shows the single time-step trips. Dashed green arrows are the outgoing segments from the origin 9g3w6 in the interval 6:00–9:00, and dashed red arrows

are the incoming segments to destination 9g3w0 in the interval 9:00–12:00. Here we see, in contrast to the previous case, two indirect paths that contribute simultaneously to the higher effective distance of the OD pair.

Instead of the same time-elapsed interval at a different quantile, in figure 7c we look at a later, but overlapping time-elapsed interval, 09:00–12:00–15:00, on the same day, quantile above 0.95. We notice several non-neighboring OD pairs have joined the mentioned pair in the high effective distance set. This alerts us to the possibility of time-based persistence in effective distances. Combined with the spatial persistence, this is a strong indication that effective distance could be examined at different scales of persistence, scale being a topic of some interest in mobility research [5, 23]. The recurrences over the course of days and over the span of a day at successive time-elapsed intervals in the general and the globally-unconnected cases, implies that there is a long-term persistence in such OD pairs, which may yield interesting flow analytical properties [24] and be amenable to space and time based topological analysis. In both time-plots, we see very high effective distances that occur infrequently, sometimes only once. It would be interesting to understand if and when, and under what conditions, such anomalous values happen, but that may require involving other information beyond the scope of this work.

5. Time-elapsed return-to-origin (RTO) distance, time, and speed

As a proxy for radius of gyration, we can calculate the travel distance (time) by a PEP to return to their origin (RTO), within a window of time-steps long enough to be sufficient. This is a special case of the time-elapsed OD distance traveled from the previous section: when the origin is also the destination. We average the RTO over all the origins, weighted by the relative probabilities of a PEP starting at them. By averaging over the origins, the RTO distance and time become intrinsic measures of the movement patterns of the community or geography to which they are associated.

5.1. *Derivation.* Setting $i = j$ in equation (4), we obtain the mean RTO distance for the path that starts at j and that returns to j between $t_1 \leq t \leq t_2$,

$$\bar{x}_{jj}^{t_1, t_2} = \frac{\sum_{t=t_1}^{t_2} x_{jj}^t \pi_{jj}^t}{\sum_{t=t_1}^{t_2} \pi_{jj}^t}.$$

Mean RTO distance for location j , for $1 \leq t \leq t_2$, excluding the first self-transition at time-step $t = 1$, is

$$\bar{x}_{jj}^{2, t_2} = \frac{\sum_{t=2}^{t_2} x_{jj}^t \pi_{jj}^t}{\sum_{t=2}^{t_2} \pi_{jj}^t}.$$

To find the overall mean of RTOs for all $j \in C$, we consider the distribution of users that leave their origins, or *roam*, instead of all the users at each origin. This distribution at time-step $t = 1$ is

$$p_j^r = \frac{\sum_{i|i \neq j} f_{ij}^1}{\sum_{i|i \neq j} f_{ij}^1}.$$

Taking the mean over the initial distribution $\{p_j^r\}$, the overall mean RTO distance excluding the first self-transition, the *roaming* RTO distance, is

$$\bar{x}^r = \sum_j p_j^r \bar{x}_{jj}^{2, t_2}.$$

Including the first self-transition, the mean RTO distance for location j is

$$\bar{x}_{jj}^{1,t_2} = \frac{\sum_{t=1}^{t_2} x_{jj}^t \pi_{jj}^t}{\sum_{t=1}^{t_2} \pi_{jj}^t}.$$

Taking the appropriate mean over the initial user distribution over the origin locations, we can get the overall mean RTO distance including the first self-transition. We estimate the initial user distribution. The probability, p_j , of a generic user being at location j at the beginning of time-step $t = 1$ was estimated in equation (3) as

$$p_j^1 = \frac{\sum_i f_{ij}^1}{\sum_{i,j} f_{ij}^1}.$$

Then, the mean RTO distance including the first self-transition, the *generic* RTO distance, is

$$\bar{x} = \sum_j p_j^1 \bar{x}_{jj}^{1,t_2}.$$

The third and simplest case is the mean RTO distance when only the first self-transition is considered, i.e., the users that are *home* in the vicinity of the location. The relative distribution of such users over all the origins at time-step $t = 1$ is

$$p_j^h = \frac{f_{jj}^1}{\sum_j f_{jj}^1}.$$

Then, the mean RTO distance of such users, the *home* RTO distance, is

$$\bar{x}^h = \sum_j p_j^h \bar{x}_{jj}^{1,2} = \sum_j p_j^h d_{jj}^1$$

where d_{jj}^1 are the (median) distances traveled at time-step $t = 1$, while self-transitioning at j .

5.2. *Results.* We calculate and plot the RTO distances for Mexico (Mexico City and surrounding region), Indonesia (Jakarta and surrounding region) and India (Mumbai and surrounding region). We do not include Colombia, for which only the data from November–December 2019 is available. In the plots we identify these regions with the city names: Mexico City, Jakarta, and Mumbai. For each country, the calculations are the averages for the time-elapsed intervals 6:00–(–)–21:00 and 9:00–(–)–00:00, weighted by the appropriate initial total trip-counts for the locations and intervals. Before we show the RTO calculations, we show the maximal component sizes in figure 8,¹⁷ which give an idea of the movement patterns in these cities. The component sizes of Mexico are much higher than India, implying movements further away in Mexico. In the calculations of RTO, these observations are seen from the point of view of a PEP’s daily movements.

¹⁷There is a missing point on the plot on 10-22-2019. The data on that date was corrupted and had to be omitted. All the subsequent time-plots are also missing that date.

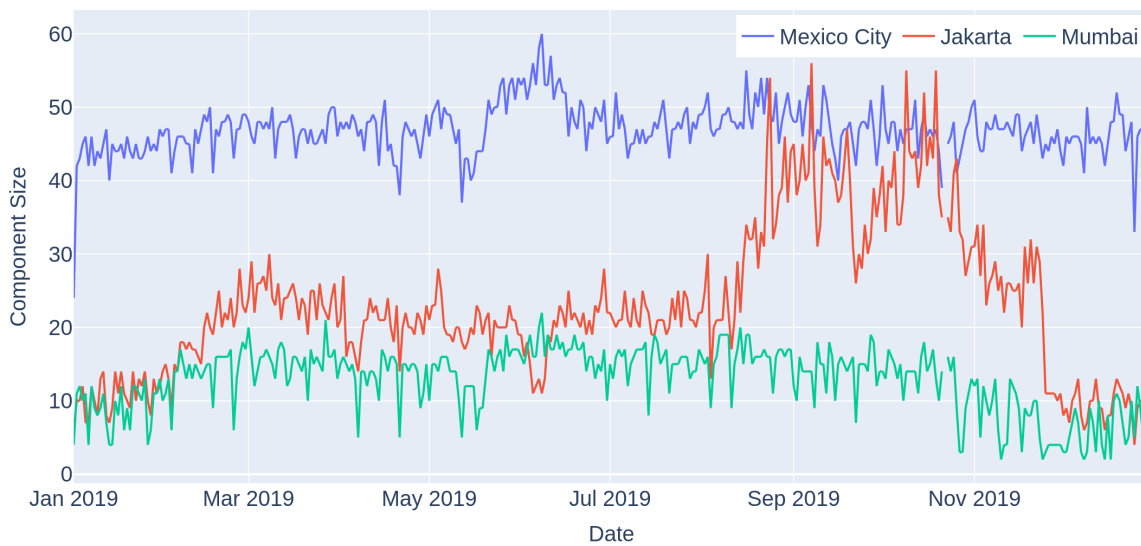


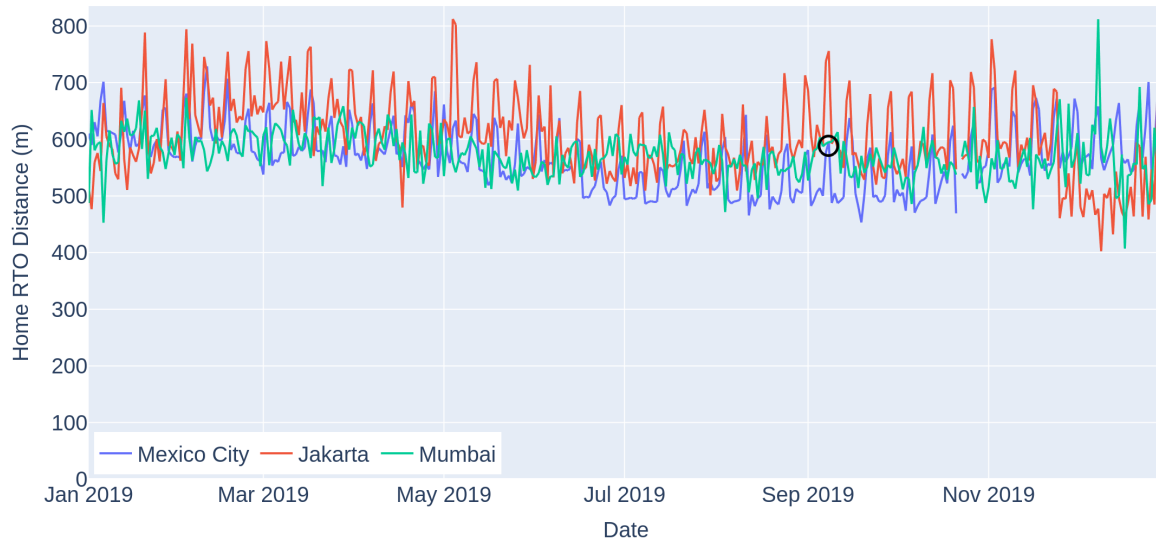
Figure 8. Mexico City, Jakarta, Mumbai: maximal component sizes.

5.2.1. *RTO distance.* In figures 7a, 7c, we plot the mean RTO *distances* against dates in 2019, for two contrasting cases. Figure 5a shows the RTO distances for the self-transitions, i.e., restricting the travel to be exactly one time-step: the *home* RTO distance. Figure 7a shows the RTO distances when the self-transitions are excluded, i.e., the PEP has to wander away before returning to the origin: the *roaming* RTO distance. They are an order of magnitude different as the former are sub-kilometer, while the latter are several kilometers.¹⁸ An interesting observation is that the home RTO distances for all the countries in figure 5a show peaks over the weekends and the roaming RTO distances in figure 7c show dips. This could be because of mostly moving in the vicinity over the weekends and commuting to work during weekdays. An instance of each of these peaks and dips for Mexico City is circled in black for 09-08-2019, which is a Sunday. Over the course of the year, we observe what might be seasonal effects on RTO distances as well.

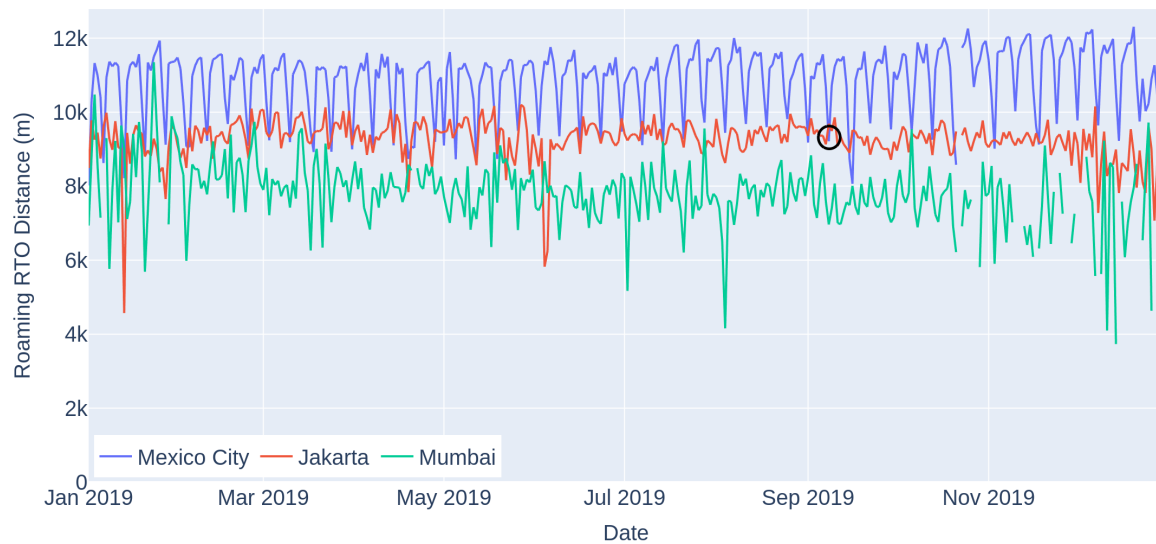
From figure 9a, PEPs in Mexico, Indonesia and India seem to have similar home distances, whereas in figure 9b, the PEP in Mexico covers a longer roaming RTO distance than a PEP in India, with that in Indonesia somewhere between the two. This could imply longer commutes in Mexico for work than in India, and Indonesia in the middle. Before March and after October, India has a sharp drop in roaming RTO distance. This could be attributable to the very small maximal component size or seasonal effects on mobility.¹⁹

¹⁸The roaming RTO distance for a region has a missing point on days when that region's maximal component size drops to 1 for the time intervals under consideration. Similarly for the roaming RTO times and speeds.

¹⁹The weekly approximate periodicity or lack thereof is due to the same in the trip-distances from which the RTO distance is calculated.



(a)

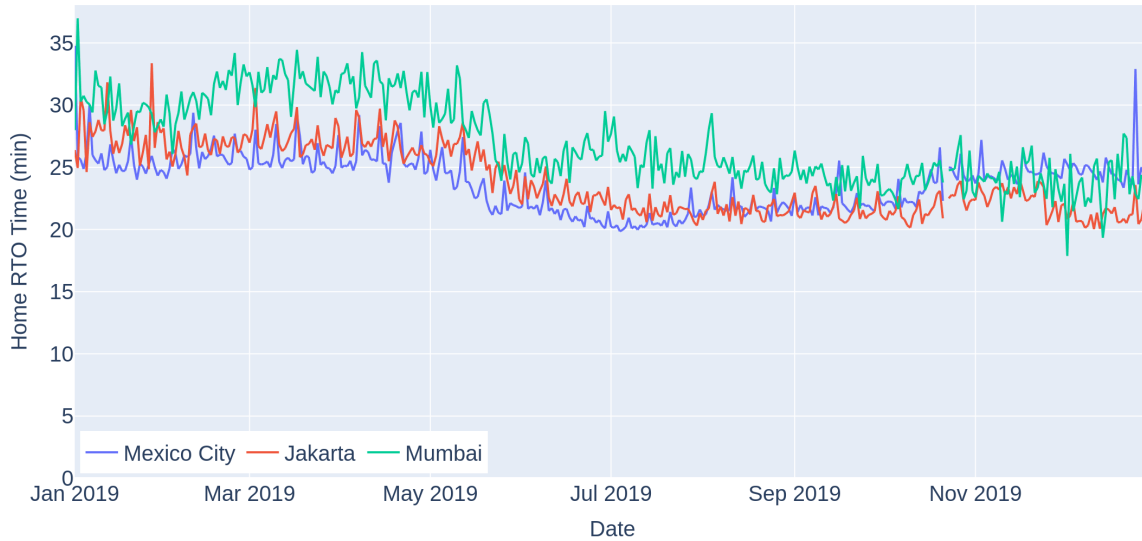


(b)

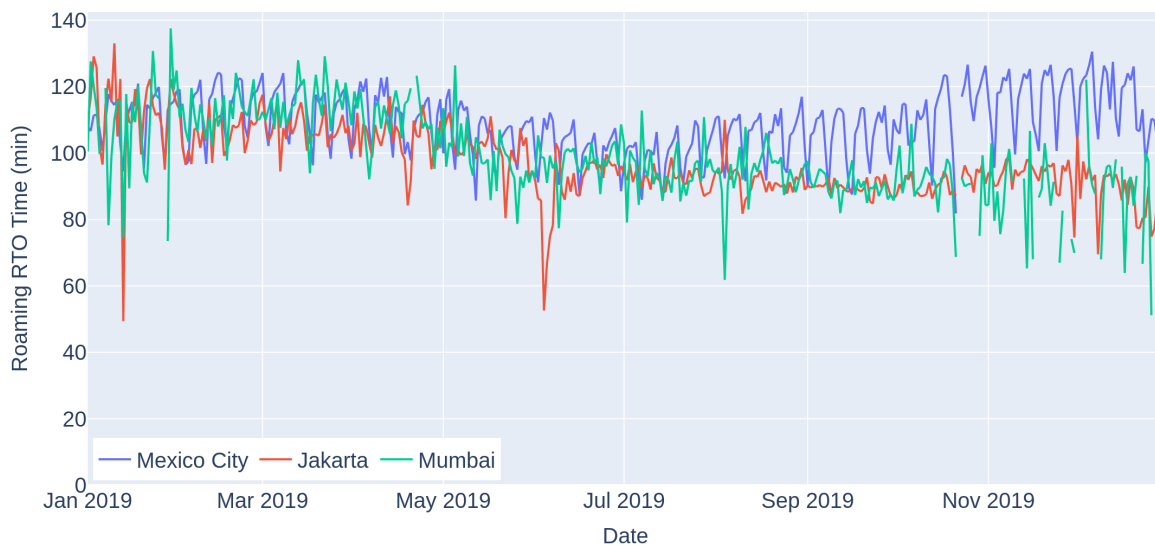
Figure 9. Mexico City, Jakarta, Mumbai (a) home RTO distances. Circled: Mexico City has a peak on Sunday, 09-08-2019. (b) roaming RTO distances. Circled: Mexico City has a dip on Sunday, 09-08-2019.

5.2.2. *RTO time.* In figures 10a, 10b, we plot the mean RTO times against dates in 2019, for the same cases as in figures 7a, 7c, applying the same designations *home* and *roaming*, respectively. These compare differently to the RTO distances. Home RTO time of India is higher than that of Mexico and Indonesia, which are similar in general. Roaming RTO time of Mexico is the highest with Indonesia the least, and India in the middle, with the trend getting more pronounced in the later half of the year.

Together, the distance and time RTOs say that a PEP in the home region in India spends more time traveling than a PEP in Mexico or Indonesia. In comparison, a roaming PEP in Mexico goes a considerably longer distance than a roaming PEP in India and takes a longer time, with Indonesia in between in distance and closer to India in time, but the proportions look different. To interpret this better, we need data on trip speeds, which we do not have direct access to in this dataset, but we create a notion of speed nonetheless from the RTO distances and times.



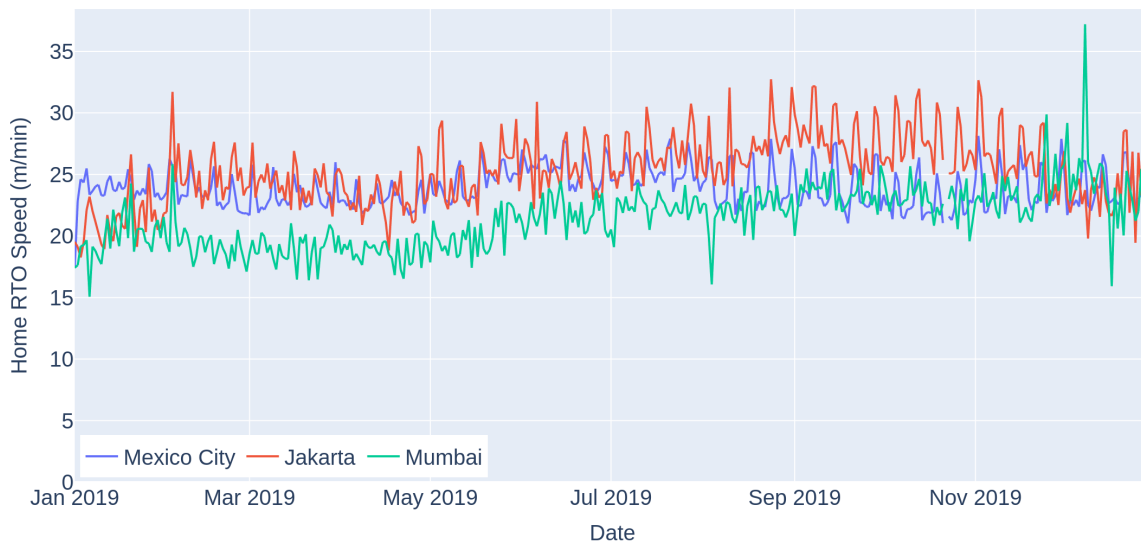
(a)



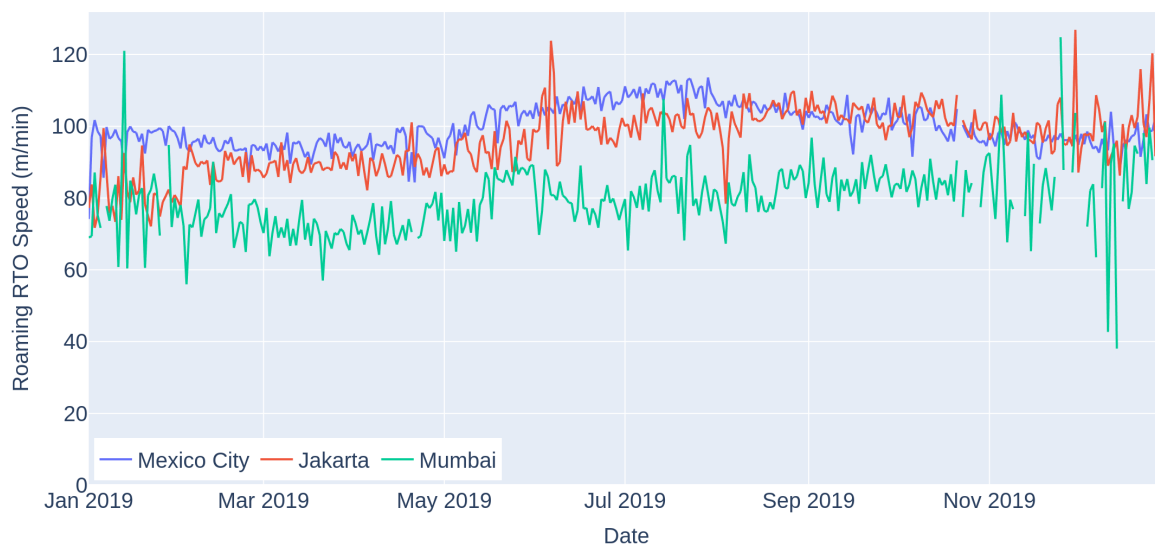
(b)

Figure 10. Mexico City, Jakarta, Mumbai (a) home RTO times (b) roaming RTO times.

5.2.3. *RTO speed*. We can combine the RTO distances and times to get the RTO *speeds*. We define RTO *speed*, as a means of comparison among the cities, to be the RTO distance traveled divided by the RTO travel time.²⁰ Figures 11a, 11b show thus defined home and roaming RTO speeds.



(a)



(b)

Figure 11. Mexico City, Jakarta, Mumbai (a) home RTO speeds (b) roaming RTO speeds.

²⁰This is a bold definition of speed because the mean of ratios is not the ratio of means. Perhaps it should be called pseudo-speed.

Home RTO speed, from the plot in figure 11a, for Indonesia is the highest and India the lowest, with Mexico being closer to Indonesia during the first half of the year and to India in the second half. In roaming RTO speed, from figure 11b, Mexico is the highest of the three, and India the lowest, and Indonesia closer to Mexico. Toward the beginning and the end of the year, Indonesia and India seem to be similar in both home and roaming speeds.

We can try to identify some of the factors at work here based on published data. Slower speeds in India would be consistent with the population density of the countries. According to data from World Bank Group collected in 2022, the population density of Mexico is approximately 66 people per square kilometer, of Indonesia about 147 people per square kilometer and of India about 479 people per square kilometer [25]. On the other hand, comparing the most populous cities of Indonesia, India and Mexico, (Jakarta, Mumbai and Mexico City, respectively), according to data from the United Nations Human Settlements Programme collected in 2020, the percentage of the population of Mexico City with convenient access to public transport is 43.3% , that of Jakarta is 54.4%, whereas that of Mumbai is 80.9% [26]. This might make up for effects of differing population densities. The exact relationship between movement speeds and other variables would have to be studied further.

6. Conclusion

In this paper we addressed the outstanding problem of estimating longer-term mobility from space and time aggregated collective data. Starting with the pseudo Markov-chain model, we developed measures and algorithms for time-elapsed net trip-counts (flow) between OD pairs, time-elapsed distance and *effective distance* and return-to-origin (RTO) distance, time and speed.

Despite the mobility-aliasing concern due to the longer intervals used for aggregation in the data we have available, the Netmob 2024 dataset, we demonstrate the measures. First validation is that of the time-elapsed OD net trip-counts (net flows) and the results we get are consistent with the expected commuting behaviors. With more detailed data and over longer time periods, it might show cycles of migration in societies.

Time-elapsed OD effective distance seems to have persistence over both space and time. This points to an additional direction of study, in which they could be used to identify recurring patterns in effective distances that are higher than expected, and an invitation to extend the time-elapsed measures to different spatio-temporal scales, study their topological properties, and develop further measures that may identify them by flow-like properties. Anomalous values of effective distances could present opportunities to investigate other datasets for explanations and to develop algorithms that identify them.

Return-to-origin (RTO) distance, time and speed calculations are a first-order characterization of the socio-economic activity rooted in geographical areas. Their variation over different geographical areas and environmental conditions over time have the potential to be useful in analyzing community level organization and behaviors, economic activity, efficiency, and even resilience in times of shocks.

At larger scales in space and time and with rich enough data, this collection of tools would potentially be useful in showing population migration, or the impact of weather or economic events on population movements. They could be combined with other geographical or demographic, social, and economic data, for example, to serve as sources for analyses to draw deeper inferences or as the ground truth for validation and prediction. To make the model closer to the actual dynamics of movement, constraints would be needed that may not

agree with the pseudo-Markov model and might add complexity or time-dependence in the model structure, or may need a generalization of the model. Seasonal variations occurring in social structures take a prominent role in the anthropological texts dealing with human history and social organizations [27], and links to mobility flows and persistence, among other measures, might help uncover patterns or discern among them.

In the context of the Netmob 2024 dataset, an application would be to glean large scale drift of people. Among the Sustainable Development Goals [28] that could be within the scope of future work, once relevant data are included, are SDG 8 – Decent work and economic growth, SDG 9–Industry, innovation and infrastructure, SDG 11 – Sustainable cities and communities, and SDG13 – Climate action.

ACKNOWLEDGEMENTS

The authors would like to acknowledge productive participation from the members of David Meyer’s research group, in particular, Itai Maimon for initiating the discussion that led to the return-to-origin definition, Orest Bucicovschi, David Rideout and Jiajie Shi.

REFERENCES

- [1] Y. de Montjoye, S. Gambs, V. Blondel, G. Canright, N. de Cordes, S. Deletaille, K. Engø-Monsen, M. Garcia-Herranz, J. Kendall, C. Kerry, G. Krings, E. Letouzé, M. Luengo-Oroz, N. Oliver, L. Rocher, A. Rutherford, Z. Smoreda, J. Steele, E. Wetter, A. Pentland, and L. Bengtsson, *On the privacy-conscious use of mobile phone data*, *Scientific Data* **5** (2018), no. 1. doi:10.1038/sdata.2018.286.
- [2] C. Buckee, S. Balsari, J. Chan, M. Crosas, F. Dominici, U. Gasser, Y. Grad, B. Grenfell, M. Halloran, M. Kraemer, M. Lipsitch, C. Metcalf, L. Meyers, T. Perkins, M. Santillana, S. Scarpino, C. Viboud, A. Wesolowski, and A. Schroeder, *Aggregated mobility data could help fight COVID-19*, *Science* **368** (2020), no. 6487, 145-146. doi:10.1126/science.abb8021.
- [3] D. Kondor, B. Hashemian, Y. de Montjoye, and C. Ratti, *Towards Matching User Mobility Traces in Large-Scale Datasets*, *IEEE Transactions on Big Data* **6** (2020), no. 4, 714-726. doi:10.1109/TBDDATA.2018.2871693.
- [4] F. Xu, Z. Tu, Y. Li, P. Zhang, X. Fu, and D. Jin, *Trajectory Recovery From Ash: User Privacy Is NOT Preserved in Aggregated Mobility Data*, *Proceedings of the 26th International Conference on World Wide Web*, 2017, pp. 1241–1250. doi:10.1145/3038912.3052620.
- [5] M. González, C. Hidalgo, and A. Barabási, *Understanding individual human mobility patterns*, *Nature* **453** (2008), 779-782. doi:10.1038/nature06958.
- [6] H. Barbosa, M. Barthelemy, G. Ghoshal, C. James, M. Lenormand, T. Louail, R. Menezes, J. Ramasco, F. Simini, and M. Tomasini, *Human mobility: Models and applications*, *Physics Reports* **734** (2018), 1-74. doi:10.1016/j.physrep.2018.01.001.
- [7] B. Jiang, J. Yin, and S. Zhao, *Characterizing the human mobility pattern in a large street network*, *Phys. Rev. E* **80** (2009), 021136. doi:10.1103/PhysRevE.80.021136.
- [8] D. Brockmann, L. Hufnagel, and T. Geisel, *The scaling laws of human travel*, *Nature* **439** (2006), no. 7075, 462-465. doi:10.1038/nature04292.
- [9] W. Zhang, M. Nunez del Prado, V. Gauthier, and S. Milusheva, *The NetMob2024 Dataset: Population Density and OD Matrices from Four LMIC Countries* (2024). doi:10.48550/arXiv.2410.00453.
- [10] N. Williams, T. Thomas, M. Dunbar, N. Eagle, and A. Dobra, *Measures of Human Mobility Using Mobile Phone Records Enhanced with GIS Data*, *PLOS ONE* **10** (2015), no. 7, 1-16. doi:10.1371/journal.pone.0133630.
- [11] C. Yang, H. Sutrisno, A. Chan, H. Tampubolon, and B. Wibowo, *Identification and Analysis of Weather-Sensitive Roads Based on Smartphone Sensor Data: A Case Study in Jakarta*, *Sensors* **21** (2021), no. 7. url:www.mdpi.com/1424-8220/21/7/2405.
- [12] Y. Yang, A. Pentland, and E. Moro, *Identifying latent activity behaviors and lifestyles using mobility data to describe urban dynamics*, *EPJ Data Science* **12** (2023), no. 1, 2193-1127. doi:10.1140/epjds/s13688-023-00390-w.
- [13] T. Wang, Y. Li, I. Chuang, W. Qiao, J. Jiang, and L. Beattie, *Evaluating the 15-minute city paradigm across urban districts: A mobility-based approach in Hamilton, New Zealand*, *Cities* **151** (2024), 105147. doi:10.1016/j.cities.2024.105147.
- [14] S. Milusheva, E. zu Erbach-Schoenberg, L. Bengtsson, E. Wetter, and A. Tatem, *Understanding the Relationship between Short and Long Term Mobility*, *AFD Research Paper Series* **2017-69** (2017).
- [15] C. Balzotti, Bragagnini A., Briani M., and E. Cristiani, *Understanding Human Mobility Flows from Aggregated Mobile Phone Data*, *IFAC-PapersOnLine* **51** (2018), no. 9, 25-30. doi:10.1016/j.ifacol.2018.07.005.
- [16] C. Peng, X. Jin, K. Wong, M. Shi, and P. Liò, *Collective Human Mobility Pattern from Taxi Trips in Urban Area*, *PLOS ONE* **7** (2012), no. 4, 1-8. doi:10.1371/journal.pone.0034487.
- [17] B. Guo, H. Yang, H. Zhou, Z. Huang, F. Zhang, L. Xiao, and P. Wang, *Understanding individual and collective human mobility patterns in twelve crowding events occurred in Shenzhen*, *Sustainable Cities and Society* **81** (2022), 103856. doi:10.1016/j.scs.2022.103856.
- [18] M. Flores-Garrido, G. de Anda-Jáuregui, P. Guzmán, A. Meneses-Viveros, A. Hernández-Álvarez, E. Cruz-Bonilla, and M. Hernández-Rosales, *Mobility networks in Greater Mexico City*, *Scientific Data* **11** (2024), 84. doi:10.1038/s41597-023-02880-y.
- [19] *NetMob 2024*. url:netmob.org.

- [20] T. Yabe, M. Luca, K. Tsubouchi, B. Lepri, M. Gonzalez, and E. Moro, *Enhancing human mobility research with open and standardized datasets*, *Nat Comput Sci* **4** (2024), 469-472. doi:10.1038/s43588-024-00650-3.
- [21] J. Norris, *Markov Chains*, Cambridge Series in Statistical and Probabilistic Mathematics, Cambridge University Press, New York, 1997. doi:10.1017/CBO9780511810633.
- [22] U. Fugacci, S. Scaramuccia, F. Iuricich, and L. Floriani, *Persistent Homology: a Step-by-step Introduction for Newcomers*, Smart Tools and Apps for Graphics - Eurographics Italian Chapter Conference, 2016. doi:10.2312/stag.20161358.
- [23] L. Alessandretti, U. Aslak, and S. Lehmann, *The scales of human mobility*, *Nature* **587** (2020), no. 7834, 402-407. doi:10.1038/s41586-020-2909-1.
- [24] X. Chen and J. Lai, *Detecting abnormal crowd behaviors based on the div-curl characteristics of flow fields*, *Pattern Recognition* **88** (2019), 342-355. doi:10.1016/j.patcog.2018.11.023.
- [25] World Bank Group, *Population density (people per sq. km of land area)*, *World Bank Open Data* (2022). url:data.worldbank.org/indicator/EN.POP.DNST?view=map.
- [26] United Nations Human Settlements Programme, *Urban Transport, UN-Habitat Urban Indicators Database* (2024). url:data.unhabitat.org/pages/urban-transport.
- [27] D. Graeber and D. Wengrow, *The dawn of everything: a new history of humanity*, Farrar, Straus and Giroux, New York, 2021. WorldCat:1255689164.
- [28] *Sustainable Development Goals*. url:undp.org/sustainable-development-goals.
- [29] N. Higham and L. Lin, *On p th roots of stochastic matrices*, *Linear Algebra and its Applications* **435** (2011), no. 3, 448-463. doi:10.1016/j.laa.2010.04.007.
- [30] E. Deza and M. Deza, *Encyclopedia of Distances*, Springer-Verlag, Berlin, 2009. doi:10.1007/978-3-642-00234-2.

APPENDIX A. Proposed data collection method and algorithmic Markov matrix resampling to compensate for mobility aliasing

The time-resolution of data could be improved by changing the intervals of data aggregation to be shorter, commensurate with a statistically useful measure of speed, perhaps a standard deviation above the mean speed. Suppose that speed is known and translates to an interval time of T minutes. The aggregation would record the trips that start in an interval mT to $(m+1)T$ and end in an interval nT to $(n+1)T$. For each m and origin there will only be finitely many n and destinations. The record would thus be indexed by the OD pair and m and n (equivalently mT and nT), a quadruple of indices, and include as data quantities of interest like trip-count, the mean (or median) time and distance traveled. The mean/median for the traveled time would likely be longer than the interval and those for distance could be shorter or longer than the spatial resolution of the geohash. This approach, while not eliminating mobility-aliasing, would help reduce it.

In the present case, the time-resolution, as noted, is coarser than needed, and potentially leads to aliasing in user and trip counts. To account for the aliasing, we could try the following idea. Continuing with the example of 3-hour, GH5, we assume that the dynamics of movements are slowly changing, at 3-hour intervals. For each coarse time-step, we need to insert p transition matrices, one for each finer interval, such that their product is the original transition matrix. Denote by H_k the finer-resolution transition matrices where $k = 1, \dots, p$. Omitting the superscript t for the original time-step, and writing $M = M^t$,

$$M = \prod_{k=1}^p H_k.$$

A more stringent version of this is if all the finer resolution matrices are assumed to be the same, i.e., $H_k = H$. Then

$$M = H^p.$$

Such a stochastic matrix H is called the p -th root of a stochastic matrix M . It might not exist, however, and finding one is a challenge [29].

An approximation might be attempted in finding the p -th root, in some distance of distance-like measure. Let the measure be K . The optimal approximation to the root would correspond to the minimum distance achievable over the space of stochastic matrices. Let the minimum distance be K_{\min} :

$$K_{\min} = \min_{B: B \text{ stochastic}} K(M, B^p).$$

Then the optimal approximation is \hat{H} such that:

$$K(M, \hat{H}^p) = K_{\min}.$$

Among such measures could conceivably be the Relative Entropy (Kullback-Leibler divergence) or the Frobenius distance [30]. The authors have not been able to find fast converging algorithms for the approximation for the size of stochastic matrices in this paper.

In summary, we would need to iterate p times the approximate stochastic p -th root of the 3-hourly transition matrix, where p is the number of shorter steps in the 3-hour interval. For instance, $p = 4$ if the shorter interval is 45 minutes. The reason for choosing the approximate p -th root is so that the transition probabilities at the 3-hour interval are consistent with it. We expect it to yield different estimates for the distance and time measures that we have

developed than those using the 3-hourly transition matrix, for the reason that mean trip-distance and trip-times are additive over path segments.